



Numerical approach-based simulation to predict cerebrovascular shear stress in a blood-brain barrier organ-on-a-chip

Sehoon Jeong^{a,b,c,1}, Jae-Hyeong Seo^{d,1}, Kunal Sandip Garud^d, Sung Woo Park^c, Moo-Yeon Lee^{d,*}

^a Department of Healthcare Information Technology, Inje University, Gimhae, 50834, Republic of Korea

^b Department of Information Communication System, Inje University, Gimhae, 50834, Republic of Korea

^c Paik Institute for Clinical Research, Inje University, Busan, 47392, Republic of Korea

^d Department of Mechanical Engineering, Dong-A University, Busan, 49315, Republic of Korea

ARTICLE INFO

Keywords:

BBB-on-a-chip
Blood-brain barrier
Microfluidic system
Organ-on-a-chip
Shear stress

ABSTRACT

Most of the compounds are impermeable to the blood-brain barrier (BBB), which poses a significant challenge in the development of therapeutics for the treatment of neurological diseases. Most of the existing *in vitro* BBB models are not capable of mimicking the *in vivo* conditions and functions. The numerical approach-based simulation model was proposed to accurately predict the *in vivo* level shear stress for the microfluidic BBB-on-a-chip. The *in vivo* level shear stress was predicted for various conditions of volume flow rates, porosities of the polycarbonate membrane of the BBB model, and dimensions of the microfluidic channel. The *in vivo* shear stress of the microfluidic BBB model increased with a decrease in the dimension of the microfluidic channel and a decrease in the porosity. The *in vivo* shear stress predicted by the optimized numerical approach-based simulation was validated within 2.17% error with the experimental *in vivo* level of shear stress at the porosity of 0.01% and all volume flow rates. The shear stress value, according to the volume flow rate of the microfluidic BBB chip with the optimal microfluidic channel size, was effective for the successful formation of tight junctions in primary endothelial cell culture. In this regard, the proposed method provided a standard for the development of various microfluidic organ-on-chip devices that replicate the *in vivo* conditions and shear stress.

1. Introduction

The blood-brain barrier (BBB) is the dynamic interface between the brain and blood. This regulates the inflow and outflow of biological substances necessary for nerve function and the metabolism of the brain. The endothelium is characterized by the presence of tight junctions. The tight junctions between brain endothelial cells form a diffusion barrier that excludes the entry of most blood mediators into the brain and protects them from systemic effects mediated by substances of any size or polar molecule compounds. Transport of nutrients from the peripheral circulation to the brain requires translocation through the endothelium by a special carrier-mediated transport way (Abbott et al., 2006; Palmiotti et al., 2014).

Cerebrovascular endothelial cells that makeup blood vessels *in vivo* are constantly affected by fluid shear stress due to normal and altered blood flow patterns. Hemodynamic forces have important effects on

many aspects of endothelial cells in maintaining normal vascular wall function. When the endothelium is exposed to physiological shear stress, it can properly differentiate and maintain the BBB phenotype. Shear stress increases the volume of endothelial cells and also regulates the physiological response to enriching microfibers and intracellular vesicles compared to cells cultured under static conditions (Ballermann and Ott 1995). There is evidence that shear stress plays an important role in regulating the production of vascular active substances, enhancing cell adhesion, improving barrier adhesion through the expression of tight junctions, cell survival, energy metabolism, and cell polarization (Buga et al., 1991; Colgan et al., 2007; Grabowski et al., 1985; Moore et al., 2010; Ott and Ballermann 1995; Tarbell 2010). Shear stress to vascular endothelial cells affects a wide range of mechano-sensors, such as ion channels, integrins, G-proteins (Ando and Yamamoto 2009). These cellular mechano-sensors with physical stimuli generated by shear stress induce activation of multiple modulators of cell physiology such as

* Corresponding author.

E-mail address: mylee@dau.ac.kr (M.-Y. Lee).

¹ Co-first authors.

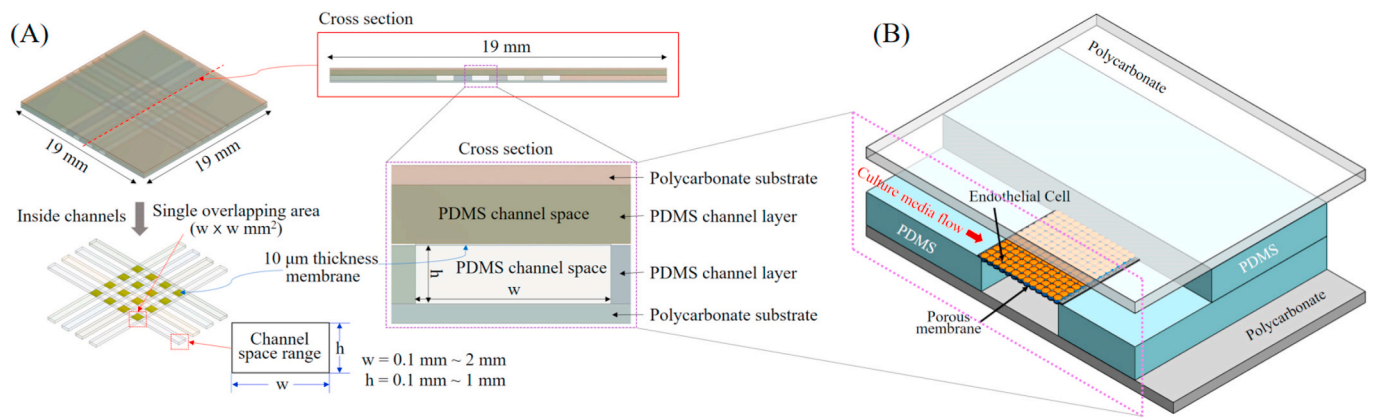


Fig. 1. (A) The geometry design domain for the microfluidic channel arrays (B) 3D structure of a single BBB unit of the BBB chip.

extracellular signal-regulated kinase 1/2-ERK1/2 (Chrétien et al., 2010). Moreover, endothelial integrity and regrowth following injury were found to be affected by fluid shear stress (Bussolari et al., 1982; Cucullo et al., 2011; Dewey et al., 1981).

Recently, *in vitro* organ-on-chips have been developed to more accurately mimic *in vivo* physiological conditions that create multicellular tissue structures, combine with microfluidic systems, and consider shear stress. A large gap remains in the physiological function that can be achieved by these *in vitro* systems compared to *in vivo* systems. It is not enough to implement a cerebrovascular system that reflects the actual shear stress because it is applied with significantly lower shear stress compared to *in vivo* (Palmiotti et al., 2014; van der Helm et al., 2016). The shear stress level of the previous *in vitro* BBB models is presented in Table S1 (Supplementary Table). Jeong et al. showed an advanced microfluidic BBB chip that recapitulates the critical functional capillary interface of the brain to importantly consider the *in vivo* shear stress level (Jeong et al., 2018).

In these cases, remarkable efforts have been addressed to develop *in vitro* organ-on-a-chip systems. Organ-on-a-chip systems are better to mimic the structural and functional units of organs, are cost-effective, and offer accurate predictions of drug efficacy and toxicity (Esch et al., 2015). However, the experimental method using *in vitro* organ-on-a-chip is still accompanied by a relatively long time. A lot of expense is involved to construct *in vivo* physiological conditions with chip fabrication, primary tissue dissociation, primary cell cultures such as endothelial cells and astrocytes.

The numerical approach-based simulation process has the main advantage of reducing the time and expense for the existing *in vitro* level research. The objective of the present study is to propose the numerical approach-based simulation model to accurately predict the *in vivo* level of shear stress for the microfluidic BBB-on-a-chip. The microfluidic BBB-on-a-chip was computationally verified with a considered experimental *in vivo* level of shear stress by systematically analyzing the shear stress value on the bottom wall of the microfluidic channel. The optimum conditions for geometrical dimensions and boundary parameters of the microfluidic BBB-on-a-chip were suggested to mimic the *in vivo* conditions and to achieve *in vivo* level shear stress with high prediction accuracy.

2. Materials and methods

2.1. Simulation process

A simulation process using a numerical approach is proposed to predict *in vivo* level shear stress in the microfluidic multi-channel BBB chip. The simulation process consists of geometry design, meshing, initial-boundary condition settings, execution of solver, and results from the analysis. Computational Fluid Dynamics (CFD) based flow analysis

was performed using ANSYS 19.1 commercial software to analyze the shear stress of the microfluidic multi-channel BBB model.

2.2. Geometry and materials

The geometry design domain of the microfluidic BBB model shows the crossed PDMS (polydimethylsiloxane) microfluidic channel arrays as shown in Fig. 1(A). The microfluidic multi-channel BBB model consists of four channels at the top and four channels at the bottom, all of which are made of PDMS material. Each channel of the BBB model is 19 mm long, the cross-sectional area of each channel is 1 mm × 300 µm (height). The channels are designed with 1 mm spacing between them. The upper channel represents the luminal channel filled with endothelial cell culture medium and the lower channel represents the abluminal channel filled with astrocyte cell culture medium. Cerebrovascular is formed on the polycarbonate membrane. The BBB unit presented in the cerebrovascular is placed at the intersection of the upper and lower channels. 16 BBB units are designed in one chip which exist in 4 × 4 parallel structures on the membrane layer. The polycarbonate membranes present in the microfluidic model have a square thickness of 10 µm and a cross-sectional area of 1 × 1 mm², which allows the liquid inside each channel to cross-move between the upper and lower channels through the polycarbonate membrane. Naturally, biomolecules in cell cultures in the upper and lower channels can migrate through the polycarbonate membrane. Endothelial cells are cultured at the top of the membrane in the cross-section (the brain blood vessel part). Astrocyte cells are cultured at the bottom of the same membrane (the brain tissue part). The two types of cells are physically isolated while simultaneously physiologically connected (Fig. 1(B)). The width of the microfluidic channel was changed from 400 µm to 2000 µm and the height of the channel was changed from 200 µm to 1000 µm to determine the optimum shear stress in the channel that may affect BBB formation. The area of the polycarbonate membrane cross-section was changed from 1 mm × 1 mm to 2 mm × 2 mm while varying the channel width from 1 mm to 2 mm to confirm the optimum shear stress value for the area of the polycarbonate membrane cross-section. The material properties of the various components of the BBB model are shown in Table S2 (Supplementary Table). The viscosity of the cell culture solution was fixed at 0.0018 Pa s (Wang et al., 2019).

2.3. Mesh and boundary conditions

The shear stress values of the microfluidic channels with five different number of mesh elements were compared to analyze mesh independence. The original geometry of the microfluidic multi-channel BBB model was 1 mm × 300 µm (height) channel cross-section and 1 mm × 1 mm × 10 µm polycarbonate membrane (Jeong et al., 2018). The mesh configuration with a tetrahedron mesh element with a body sizing

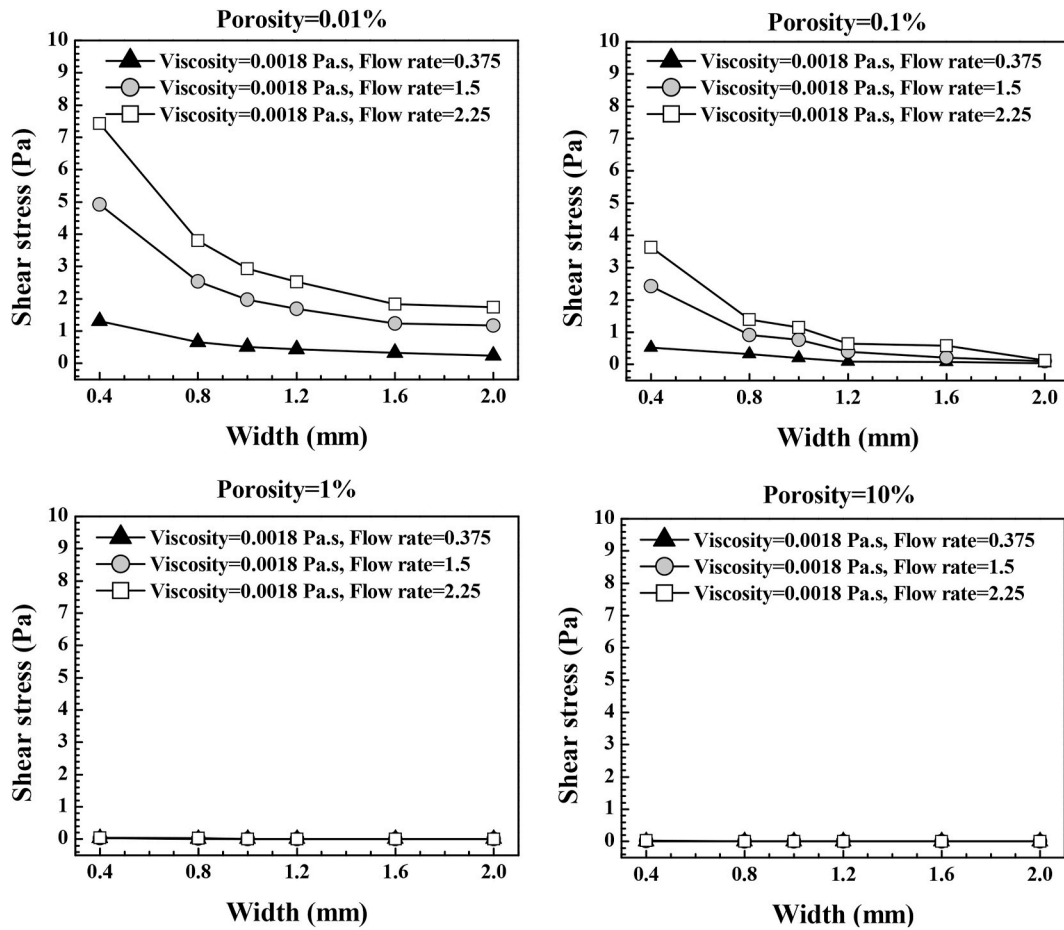


Fig. 2. Variation of shear stress to the width of the channels for various porosities, different flow rates, and viscosity of 0.0018 Pa s

of 1.3 mm was used. The volume flow rate of the internal working fluid at the channel inlet, fluid viscosity, and polycarbonate membrane porosity were considered as the boundary condition for the numerical flow analysis. The details of various boundary conditions that were used in the numerical flow analysis are presented in Table S3 (Supplementary Table). The boundary conditions in the present numerical analysis were selected based on the reported experimental conditions (Jeong et al., 2018).

2.4. Governing equations

In the solver execution step, the continuity, momentum, and energy equations as presented by Equations (2) to (4) were considered in ANSYS CFX using the finite difference method under the considerations of stated boundary conditions.

The shear stress value on the bottom wall (τ_{wall}) of a microfluidic channel was derived from the Navier–Stokes equation describing the fluidic motion inside a rectangular shaped channel (Equation (1)).

$$\tau_{wall} = \frac{6Q\mu}{wh^2} \quad (1)$$

where τ_{wall} is the shear stress, Q is the volumetric flow rate, μ is the dynamic fluid viscosity, w and h indicate the width and height of the channel, respectively.

Governing equations were discretized for the selected mesh using the finite element technique and solved for each mesh element. Equations were solved for mesh elements using various boundary conditions till solutions converge. The working fluid which mimics the culture media flowing in the multi-channel for the microfluidic BBB model was

assumed to be incompressible (Chan et al., 2007). The calculated Reynolds numbers at all geometry models and volume flow rates were below 2000. The working fluid motion through the multi-channels was assumed to be laminar. The Newtonian flow model was applied for the simulation of the microfluidic BBB model.

$$\frac{\partial \rho}{\partial t} + \nabla \cdot (\rho U) = 0 \quad (2)$$

$$\frac{\partial (\rho U)}{\partial t} + \nabla \cdot (\rho U \otimes U) = -\nabla p + \nabla \tau + S_M \quad (3)$$

$$\frac{\partial (\rho h)}{\partial t} + \nabla \cdot (\rho U h) = \nabla \cdot (\lambda \nabla T) + \tau : \nabla U + S_E \quad (4)$$

Where τ is the shear stress tensor and expressed by following relation with strain rate,

$$\tau = \mu \left(\nabla U + (\nabla U)^T - \frac{2}{3} \nabla \cdot U \right) \quad (5)$$

In Equations (2) to (5), ρ is the fluid density, t is the time, U is the fluid velocity, p is the static pressure, h is the enthalpy, λ is the fluid thermal conductivity, T is the temperature, $\tau : \nabla U$ is the viscous dissipation term, S_M and S_E are momentum source and energy source, respectively.

2.5. Primary cell culture and microfluidic culture in the BBB chip

Primary mouse brain microvascular endothelial cells derived from C57BL/6 mice were purchased and subcultured (Celprogen, CA). Primary endothelial cells were maintained in 10% FBS (Fetal Bovine

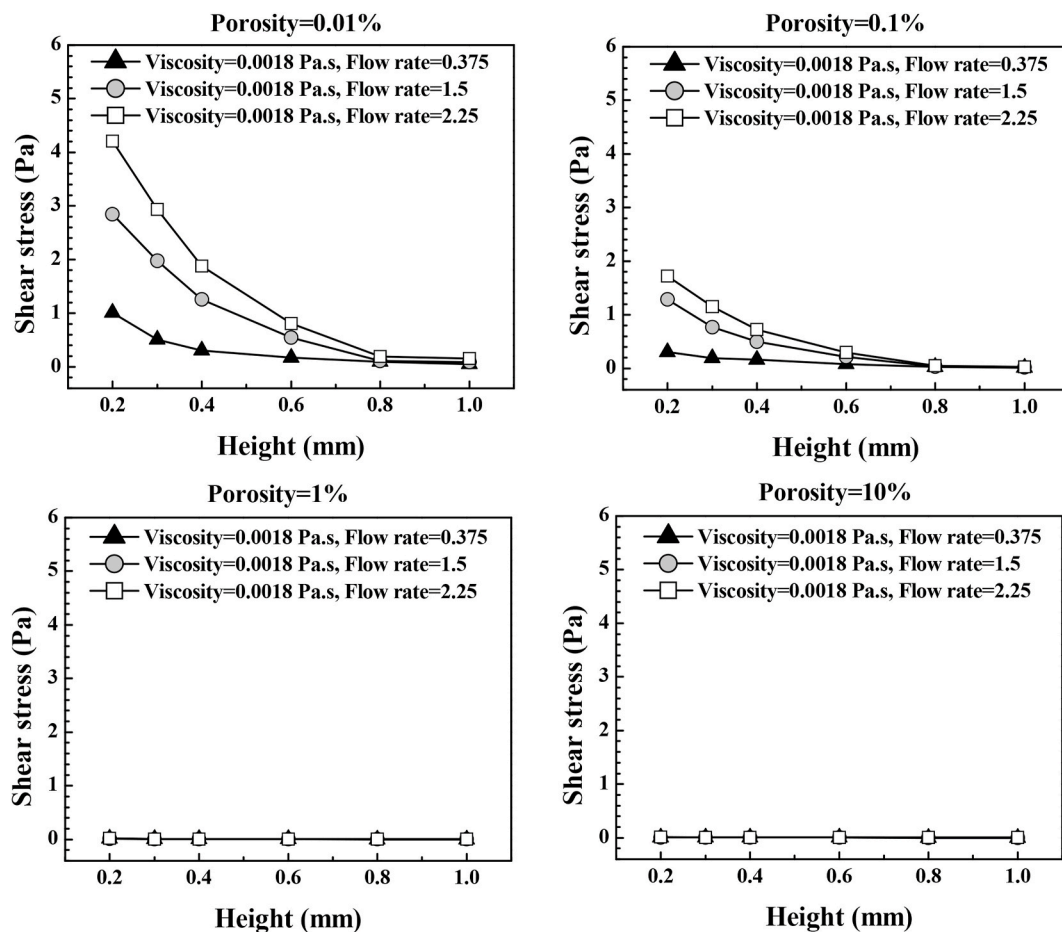


Fig. 3. Variation of shear stress to channel height for various flow rates, various porosities, and for the viscosity of 0.0018 Pa s

Serum) supplemented with IMDM (Iscove's Modified Dulbecco's Medium, Thermo Fisher Scientific, MA) containing 2.0 mM GlutaMAX (Invitrogen, CA). The BBB chip was fabricated as previously reported (Jeong et al., 2018). The PDMS layer was made of microfluidic channel arrays with width, length, and height of 1 mm, 19 mm, and 300 μm , respectively. 10% Matrigel (BD Biosciences, CA) was injected into the BBB chip to form an extracellular matrix where endothelial cells were cultured. Primary endothelial cells were seeded at a density of 150 cells/ mm^2 in the top channels of the chip. The endothelial cell culture was kept static for the cells to the channel on the chip. After 24 h, a shear stress of 20 dyne/ cm^2 to the endothelial cells was applied and the culture was continued to grow at a media flow rate of 1.5 $\mu\text{L}/\text{min}$ for 3 days. All animal procedures were approved by Inje University (Protocol #2020-015) Institutional Animal Care and Use Committee (IACUC).

2.6. Immunocytochemistry

Cells were fixed in 4% paraformaldehyde for 20 min at 25 $^{\circ}\text{C}$ and permeabilized with 0.1% Triton X-100 for 10 min at room temperature. The samples were stirred overnight at 4 $^{\circ}\text{C}$ in primary antibody: anti-zonula occludens-1 (ZO-1, mouse monoclonal, 1: 100, Life Technologies, NY) after treatment with 5% goat serum for 1 h at room temperature. The samples were then stirred at room temperature for 1 h in secondary antibody from Alexa 594 goat anti-mouse (1:1000, Life Technologies, NY). Samples were rinsed with PBS (Phosphate-Buffered Saline) after each step. ZO-1 had been used for the identification of tight junction proteins between endothelial cells. Nuclei stained with Hoechst 33342 (1 $\mu\text{g}/\text{mL}$, Life Technologies, NY) to observe the cellular morphology. Fluorescently labeled cells were imaged using an inverted

microscope (Olympus, Japan).

3. Results and discussion

3.1. Optimization of mesh setting for shear stress in the microfluidic channel geometry

As the blood flows through the brain blood vessel part, shear stress created inside the channel plays an important role in the formation of the BBB unit. It is necessary to consider the porosity of the polycarbonate membrane, the viscosity of the working fluid, the volume flow rate, and the various geometrical values of the fluid channels to reliably analyze the shear stress levels in the change of the actual physical environment. The channel length remained the same at 19 mm in all analytical models since the channel length does not affect the formation of shear stress (Jeong et al., 2018). Sellgren et al. showed that the width and height of the channel affect significantly the shear stress of the microfluidic neurovascular (cerebrovascular) unit model (Sellgren et al., 2015). Fig. S1(A)(Supplementary Figure) showed meshing results of the standard analytical model on the microfluidic multi-channel BBB model. Fig. S1(B)(Supplementary Figure) showed the mesh dependency of the shear stress values of the microfluidic multi-channel BBB model. The shear stress values showed significant variation at the mesh number from 3,494,164 to 12,158,723 elements. The shear stress values at the mesh number above 8,074,108 elements were varying within $\pm 1\%$. Hence, the meshing with about 8,000,000 elements was applied for further numerical analysis cases on the microfluidic multi-channel BBB model.

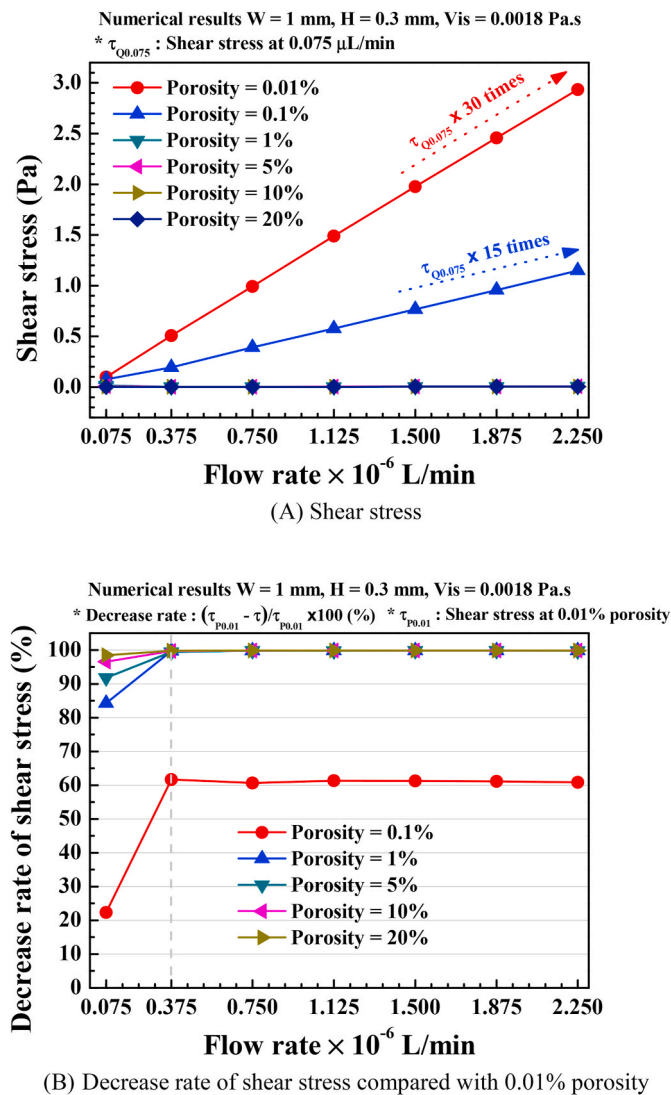


Fig. 4. The behavior of shear stress to the flow rate for different porosities ranging from 0.01% to 20%.

3.2. Boundary width of the microfluidic channel for the brain blood vessel

The relationship between microfluidic channel width and shear stress to consider the practically acceptable boundary values of the channel width range has been examined if it is assumed that an actual microfluidic BBB model has been established. The test was carried out with the porosity values fixed at four types (10%, 1%, 0.1%, 0.01%) since the intersecting part of the upper channel and the lower channel was made of a pore membrane. As shown in Fig. 2, shear stress values were tested according to the flow rate of the cell culture medium by varying the width of the microchannels by 0.2 mm from 0.4 mm to 2.0 mm. In the case of the porosity value of 10% and 1%, the width of the microchannels did not affect the shear stress value according to the flow rate of the cell culture because the shear stress values were less than 0.05 Pa in all cases.

At the porosity value of 0.01%, as we expected in Equation (1), the shear stress value was decreased by a maximum of 81.8% according to the flow rate of the cell culture while the width of the microchannels was changed from 0.4 mm to 2.0 mm. In the case of 0.1% porosity value, the shear stress value was decreased by a maximum of 96.3% according to the flow rate of the cell culture while the width of the microchannels was changed from 0.4 mm to 2.0 mm. The decrease rate of the shear stress at a width range of 0.4 mm to 1.2 mm in the case of 0.1% porosity value

was the higher maximum by 24.7% than results in the case of 0.01% porosity. However, the shear stress with the microchannel width of 1.6 mm was relatively similar to the shear stress at the width of 1.2 mm. At microchannels width of 2.0 mm, the shear stress values according to the flow rate of the cell culture were all less than 0.5 Pa. This result implies that when making actual microchannels, the boundary width value should not exceed 1.6 mm. Koutsiaris et al. proved that shear stress decreased significantly as the dimension of the channel increased (Koutsiaris et al., 2013).

3.3. Boundary height of the microfluidic channel for the brain blood vessel

The effect of the boundary height of the microfluidic channel on shear stress has been analyzed. In Fig. 3, the shear stress values were tested according to the flow rate of the cell culture medium by varying the height of the microchannel by 0.2 mm from 0.2 mm to 1.0 mm. When the porosity values were 10% and 1%, the microchannel size did not affect the shear stress value with the flow rate of the cell culture because the shear stress values in all cases were less than 0.02 Pa. At porosity values of 0.1% and 0.01%, the shear stress values with the flow rate of the cell culture were decreasing while the microchannel height changed from 0.2 mm to 0.8 mm, as expected in Equation (1).

However, in both cases of porosity values of 0.1% and 0.01%, even if the microchannel height increased from 0.8 mm to 1.0 mm, the shear stress values according to the flow rate of the cell culture were not so significant that they were very similar. This result means that when creating a real microchannel, it is recommended that the boundary height value be designed so that it does not exceed 0.8 mm. Van der Helm et al. also showed that the shear stress of the microfluidic organ-on-chip for the BBB model decreased with an increase in the width and height of the channel. And the study also concludes that the smaller height compares with width showed uniform shear stress (van der Helm et al., 2016).

3.4. Effect of the porosity in the microfluidic channel for the brain blood vessel

When the endothelial cells are cultured on the membrane and tight junctions are formed between the endothelial cells, the BBB in the cerebral vessels is formed properly. The proper formation of the BBB means that the porosity of the membrane part is low, and the collapse of the BBB means that the porosity of the membrane part is high. Fig. 4(A) shows the shear stress value of each volume flow rate according to the porosity change in the range of 0.01% to 20% to analyze the effect of the porosity change on the shear stress value in the membrane part. Analysis of the effect of polycarbonate membrane porosity on shear stress was performed on a microfluidic BBB model with a membrane part of the channel cross-section in a $1 \times 1 \text{ mm}^2$, a channel height of 0.3 mm, and a 0.01 mm polycarbonate membrane thickness (Fig. 1). Since the viscosity of the cell culture solution was 0.0018 Pa s, the viscosity was analyzed in a state where the viscosity value was fixed at 0.0018 Pa s. In Fig. 4(A), all the shear stress values with the volume flow rate of $2.25 \mu\text{L/min}$ at the porosities of 1%, 5%, 10%, and 20% decreased by 99.8% than that of the porosity of 0.01% and the shear stress value at the porosity of 0.1% decreased by 60.8% than that of the porosity of 0.01%. Shear stress values were almost zero for all volume flow changes under conditions where the porosity of the membrane ranged from 1% to 20%. On the other hand, under the condition of 0.1% and 0.01% porosity, the shear stress increased considerably as the velocity of fluid flow increased. When the volume flow rate increased from the lowest value of $0.075 \mu\text{L/min}$ to the maximum value of $2.25 \mu\text{L/min}$, the shear stress value in the microfluidic BBB model increased about 30 times at 0.01% porosity and about 15 times at 0.1% porosity. Fig. 4(B) shows the decrease rate of shear stress value of each volume flow rate according to the porosity change in the range of 0.1% to 20% compared with 0.01% porosity to

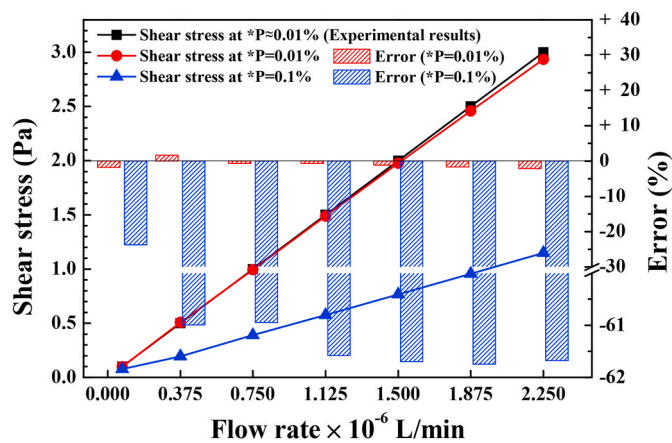


Fig. 5. Validation of shear stress values for the optimum case between numerical and experimental results. Error is $\{(\tau_{\text{Simulation}} - \tau_{\text{Experiment}}) / \tau_{\text{Experiment}}\} \times 100\%$. *P is porosity.

analyze the effectiveness of the porosity change on the shear stress value in the membrane part. The shear stress value with the volume flow rate of 0.075 $\mu\text{L}/\text{min}$ at 0.1% porosity was decreased by 22.3% compared with that at 0.01% porosity. The decrease rates of shear stress value with the volume flow rate of 0.075 $\mu\text{L}/\text{min}$ at 1%, 5%, 10% and 20% porosities were 84.3%, 91.8%, 96.5%, and 98.4% compared with 0.01% porosity. The decrease rates of shear stress value with the volume flow rates over 0.375 $\mu\text{L}/\text{min}$ at 0.1% porosity were maintained by $61.1 \pm 0.5\%$. Whereas the decrease rates of shear stress value at the volume flow rates over 0.375 $\mu\text{L}/\text{min}$ and over 1% porosities were maintained by average 99.8%. These results mean the membrane part of the channel over 1% porosities have less effect on the shear stress variation despite the increase of volume flow rate. Hernández-Gómez et al. proved that shear stress decreased as the porosity increased due to a decrease in the velocity of a fluid. The lower porosities showed high shear stress values and vice-versa (Hernández-Gómez et al., 2015).

As expected, it was also confirmed by the numerical approach-based simulation that the shear stress value increased with the blood velocity in the blood vessel. However, once the BBB collapsed, it was found that even if the porosity of the part exceeded only 1%, the shear stress did not help to form the BBB correctly.

3.5. Characteristic analysis and experimental validation

The results from the computational analysis were compared with the experimental results by Jeong et al. under the matched boundary conditions of our established microfluidic channel model (the boundary width < 1.6 mm, the boundary height < 0.8 mm) (Jeong et al., 2018). In this study, the microfluidic channel has a channel width of 1.0 mm and a channel height of 0.3 mm. The study explains that the *in vitro* BBB model is most similar to the *in vivo* BBB model than the other *in vitro* BBB models so that the drug response appears very similar to the *in vivo* BBB model. This means that when BBB is formed in the *in vitro*

cerebrovascular system, the permeability of the *in vitro* blood vessel is also significantly lower than that in an *in vivo* cerebrovascular system. Therefore, it is considered that this point has the experimental condition closest to the lowest porosity value which is set, 0.01%. The shear stress value corresponding to various flow rates used in the reference paper (Jeong et al., 2018) is shown in Table S4 (Supplementary Table). Similar conditions to the *in vivo* level shear stress applied by the previous experimental study (Jeong et al., 2018) were applied to the simulation approach we implemented, and the experimental results and our simulation results were numerically compared and analyzed. Fig. 5 shows the shear stress values of both numerical simulation and experimental study for various volume flow rates from 0.075 $\mu\text{L}/\text{min}$ to 2.25 $\mu\text{L}/\text{min}$. Based on the shear stress level used in the experiment, the error rate in the porosity 0.1% ranged from 20% to 61%, whereas the porosity 0.01% showed an error rate of approximately 2.17%.

Based on these results, primary neurovascular endothelial cells were cultured in our microfluidic BBB chip and shear stress at an *in vivo* level (20 dyne/cm^2) was applied. The cells were immunostained with antibodies to the tight junction protein ZO-1 to investigate whether primary neurovascular endothelial cells cultured in the microfluidic device form adequate tight junctions. Fig. 6(A) indicates a high expression of ZO-1 at junctions between endothelial cells, resulting in the formation of tight junctions between endothelial cells. Fig. 6(B) and (C) show the nucleus of neurovascular endothelial cells and the merged image. Through the experimental results of applying shear stress to endothelial cells, it was confirmed that the simulation analysis we studied was very helpful in making excellent experimental results even in actual experimental results. In this regard, it can be seen that applying our simulation model when implementing an *in vitro* BBB model can provide reliable prediction results with considerably similar matching when performing an actual experiment.

4. Conclusion

In the present study, the numerical approach-based simulation model was developed to accurately predict the *in vivo* level of shear stress for the microfluidic BBB-on-a-chip which was close to actual experimental results. The *in vivo* shear stress of the microfluidic BBB model increased with a decrease in the dimension of the microfluidic channel and with a decrease in the porosity of the polycarbonate membrane of the BBB chip. The optimum conditions for geometrical dimensions of the microfluidic BBB-on-a-chip were suggested to mimic the *in vivo* conditions and to achieve *in vivo* level shear stress with high prediction accuracy. Based on these optimized numerical approach-based simulation results, a real microfluidic BBB-on-a-chip was developed. For all volume flow rates, the *in vivo* shear stress predicted by the optimized numerical approach-based simulation showed an error rate of 2.17% with the experimental results at the porosity of 0.01%. Therefore, the presented method can be applied to any microfluidic organ-on-chip devices with microfluidic channels holding blood vessels that account for *in vivo* shear stress, providing a standard for various organ-on-chip development targeting *in vivo* BBB models. Planned future work could focus on the extension of the proposed numerical approach-based

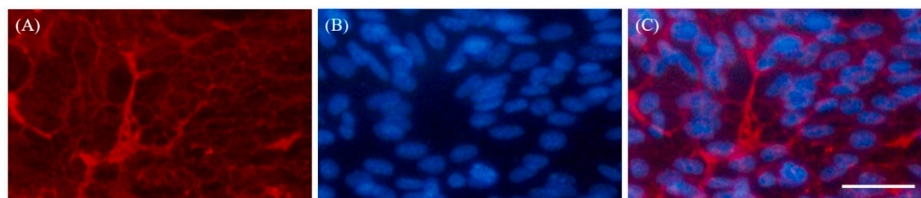


Fig. 6. Immunocytochemistry showing endothelial cell growth and formation of tight junctions using tight junction protein ZO-1 (red: ZO-1 stain for tight junction, blue: Hoechst stain for nuclei). Scale bar: 50 μm . (For interpretation of the references to colour in this figure legend, the reader is referred to the Web version of this article.)

simulation model for various blood vessels to expect an intensive effect of the drug.

CRediT authorship contribution statement

Sehoon Jeong: Conceptualization, Methodology, Validation, Formal analysis, Investigation, Resources, Data curation, Writing – original draft, Writing – review & editing, Visualization, Supervision, Project administration, Funding acquisition. **Jae-Hyeong Seo:** Conceptualization, Methodology, Software, Validation, Formal analysis, Resources, Data curation, Writing – original draft, Writing – review & editing, Visualization. **Kunal Sandip Garud:** Conceptualization, Methodology, Software, Validation, Formal analysis, Resources, Data curation, Writing – original draft, Visualization. **Sung Woo Park:** Investigation, Resources, Data curation, Writing – original draft, Visualization. **Moo-Yeon Lee:** Conceptualization, Methodology, Software, Writing – original draft, Writing – review & editing, Supervision, Project administration, Funding acquisition.

Declaration of competing interest

The authors declare that they have no known competing financial interests or personal relationships that could have appeared to influence the work reported in this paper.

Acknowledgments

This work was supported by the National Research Foundation of Korea(NRF) grant funded by the Korea government(MSIT) (No. NRF-2018R1C1B5086455, No. 2020R1A2C1011555).

Appendix A. Supplementary data

Supplementary data to this article can be found online at <https://doi.org/10.1016/j.bios.2021.113197>.

References

- Abbott, N.J., Ronnback, L., Hansson, E., 2006. *Neuroscience* 7 (1), 41–53.
- Ando, J., Yamamoto, K., 2009. *Circ. J.* 73 (11), 1983–1992.
- Ballermann, B.J., Ott, M.J., 1995. *Blood Purif.* 13 (3–4), 125–134.
- Buga, G.M., Gold, M.E., Fukuto, J.M., Ignarro, L.J., 1991. *Hypertension* 17 (2), 187–193.
- Bussolari, S.R., Dewey, C.F., Gimbrone, M.A., 1982. *Rev. Sci. Instrum.* 53 (12), 1851–1854.
- Chan, W.Y., Ding, Y., Tu, J., 2007. *ANZIAM J.* 47, 507–523.
- Chrétien, M.L., Zhang, M., Jackson, M.R., Kapus, A., Langille, B.L., 2010. *J. Cell. Physiol.* 224 (2), 352–361.
- Colgan, O.C., Ferguson, G., Collins, N.T., Murphy, R.P., Meade, G., Cahill, P.A., Cummins, P.M., 2007. *Am. J. Physiol. Heart Circ. Physiol.* 292 (6), H3190–H3197.
- Cucullo, L., Hossain, M., Puvenna, V., Marchi, N., Janigro, D., 2011. *BMC Neurosci.* 12, 40.
- Dewey Jr., C.F., Bussolari, S.R., Gimbrone Jr., M.A., Davies, P.F., 1981. *J. Biomech. Eng.* 103 (3), 177–185.
- Esch, E.W., Bahinski, A., Huh, D., 2015. Organs-on-chips at the frontiers of drug discovery. *Nat. Rev. Drug Discov.* 14 (4), 248–260.
- Grabowski, E.F., Jaffe, E.A., Weksler, B.B., 1985. *J. Lab. Clin. Med.* 105 (1), 36–43.
- Hernández-Gómez, L.H., Rangel-Elizalde, A.I., Beltrán-Fernández, J.A., González-Rebatú, A., Corro-Valdez, N., Urriolagoitia-Calderón, G., Rodríguez-Martínez, R., 2015. An optimization of the manufacturing process of corporeal screws made of synthetic bone. In: Öchsner, A., Altenbach, H. (Eds.), *Applications of Computational Tools in Biosciences and Medical Engineering*. Springer, Switzerland, pp. 43–59.
- Jeong, S., Kim, S., Buonocore, J., Park, J., Welsh, C.J., Li, J., Han, A., 2018. *IEEE Trans. Biomed. Eng.* 65 (2), 431–439.
- Koutsias, A.G., Tachmitzi, S.V., Batis, N., 2013. *Microvasc. Res.* 85, 34–39.
- Moore, J.P., Weber, M., Searles, C.D., 2010. *Arterioscler. Thromb. Vasc. Biol.* 30 (3), 561–567.
- Ott, M.J., Ballermann, B.J., 1995. *Surgery* 117 (3), 334–339.
- Palmiotti, C.A., Prasad, S., Naik, P., Abul, K.M., Sajja, R.K., Achyuta, A.H., Cucullo, L., 2014. *Pharm. Res. (N. Y.)* 31 (12), 3229–3250.
- Sellgren, K.L., Hawkins, B.T., Grego, S., 2015. *Biomicrofluidics* 9 (6), 061102.
- Tarbell, J.M., 2010. *Cardiovasc. Res.* 87 (2), 320–330.
- van der Helm, M.W., van der Meer, A.D., Eijkel, J.C.T., van den Berg, A., Segerink, L.I., 2016. *Tissue Barriers* 4 (1), e1142493.
- Wang, Z., Huang, C., Wang, J., Wang, P., Bi, S., Abbas, C.A., 2019. *Chin. J. Mech. Eng.* 32 (1), 19.